Procedia Computer Science

Volume 80, 2016, Pages 1382–1391

ICCS 2016. The International Conference on Computational Science

# Numerical aspects related to the dynamic update of anisotropic permeability field during the transport of nanoparticles in the subsurface

Meng-Huo Chen[1], Amgad Slama[2], and Mohamed El-Amin[3]

[1] King Abdullah University of Technology and Science, Thuwal, K.S.A
menghuo.chen@kaust.edu.sa
[2] Reservoir Engineering Research Institute, Palo Alto, California, U.S.A.
asas.tx@@gmail.com
[3] Effat University, Jeddah, K.S.A
mohamed.elamin.kaust@gmail.com

**Abstract**

Nanoparticles are particles that are between 1 and 100 nanometers in size. They present possible dangers to the environment due to the high surface to volume ratio, which can make the particles very reactive or catalytic. Furthermore, rapid increase in the implementation of nanotechnologies has released large amount of the nanowaste into the environment. In the last two decades, transport of nanoparticles in the subsurface and the potential hazard they impose to the environment have attracted the attention of researchers. In this work, we use numerical simulation to investigate the problem regarding the transport phenomena of nanoparticles in anisotropic porous media. We consider the case in which the permeability in the principal direction components will vary with respect to time. The interesting thing in this case is the fact that the anisotropy could disappear with time. We investigate the effect of the degenerating anisotropy on various fields such as pressure, porosity, concentration and velocities.

*Keywords:* Nanoparticle transport, multipoint flux approximation, anisotropic porous media, algebraic multigrid.

## 1 Introduction

Nanoparticles are particles that are between 1 and 100 nanometers in size. Due to their high surface to volume ratio, nanoparticles become highly reactive or catalytic and may impose a negative impact on the environment. In particular, large quantities of these materials might have already leached into our subsurface groundwater reservoirs and started to transport. On the other hand, nanomaterials have been extensively used in petroleum-related industries. They have been applied to various activities such as reservoir exploration, drilling and completion,

 Selection and peer-review under responsibility of the Scientific Programme Committee of ICCS 2016


doi:10.1016/j.procs.2016.05.440

production and improved oil recovery as well as refinery. All these raise the concern about the fate of these material in their local environment and motivate the research on the transport of nanoparticle in the environment.

# 2 Transport models of nanopartilces

To model the transport of nanoparticles we use Eulerian specification to characterize the flow fields. In this approach the nanoparticles are not tracked and one looks at fluid motion that focuses on specific locations in the space through which the fluid flows as time passes. Besides the fluid equations, a balance equation for the mass of the particles is derived. Furthermore, a filtration term is added to the advection-dispersion equation to account for nanoparticle transport and deposition process.

## 2.1 Filtration theory

Several authors have developed several filtration models to study transport of nanoparticles ([1]-[3]). Goldberg et al. [4] have reviewed a number of these models. They categorized them according to the mechanisms involved in the transport processes, including deposition(fast and slow), remobilization, and blocking. The complexity of these model vary according to the assumption considered. In addition to the conventional advection-dispersion process, the mechanisms affecting the transport of nanoparticles include retardation, detachment, site blocking and a combination of them. The general equation for advection-dispersion process in porous media may be written as:

$$\phi\frac{\partial c}{\partial t} + \nabla\cdot(\mathbf{u}c - \mathbf{D}\nabla c) = R + q_c \tag{1}$$

where $c$ is the concentration of nanoparticles, u is Darcy velocity, $\phi$ is the porosity, $\mathbf{D}$ is the dispersion tensor, $R$ accounts for mass insertion or depletion due to chemical reaction, and $q_c$ is a source/sink term. In filtration theory, the migration of the very fine particles is accompanied by deposition. This phenomena is incorporated into the governing balance equation by adding the rate at which the mass is deposited to the mass accumulation term [5], such that:

$$\frac{\partial c}{\partial t} + \frac{\rho_b}{\phi}\frac{\partial s}{\partial t} = -\nabla\cdot(\mathbf{u}c - \mathbf{D}\nabla c) + R + q_c \tag{2}$$

where $\rho_b$ represents the solid bulk density and $s$ is the concentration at the surface. The deposition rate is proportional to the concentration of nanoparticles. Denote the particle deposition coefficient as $k_{\text{dep}}$, we have

$$\frac{\rho_b}{\phi}\frac{\partial s}{\partial t} = k_{\text{dep}}c \tag{3}$$

The process of deposition of nanoparticles is assumed to be irreversible and $s$ can grow indefinitely. Depending on difference assumptions, there have been several approaches proposed by authors in order to describe various filtration scenarios. To account or possible retardation of nanoparticles, He et al. [6] proposed a model of the form:

$$\Big(1 + \frac{\rho_b k_d}{\phi}\Big)\frac{\partial c}{\partial t} = -\nabla\cdot(\mathbf{u}c - \mathbf{D}\nabla c) - k_{\text{dep}}c \tag{4}$$

where $k_d$ is the particle deposition coefficient [1/T] which depends on the flow velocity. To account for detachment of particles, Bradford et al. [3] suggested

$$-\frac{\partial \rho_b s}{\partial t} = \phi k_{\text{att}}c + \rho_b k_{\text{det}} \tag{5}$$

where $k_{\text{att}}$ [1/T] is the is the first order colloid attachment coefficient, $k_{\text{det}}$ is the first-order colloid detachment coefficient. If one considers site blocking, Cullen et al. [7] suggested that the rate of nanoparticles deposition takes the form:

$$\left(\frac{\rho_b}{\phi}\right)\frac{\partial s}{\partial t} = k_{\text{dep}}\left(1 - \frac{s}{s_{\max}}\right)c \tag{6}$$

## 2.2 Transport phenomena in anisotropic porous media

In this work we simulate the nanpparticle transport phenomena in anisotropic porous media in which case the direction of the anisotropy does not align with the grid lines. Anisotropy can be observed in almost all subsurface formation due to the several physiochemical and mechanical processes that took place over the longer geologic time scale. Cullen et al. [7] investigated the transport of carbon nanoparticles in a two dimensional heterogeneous anisotropic porous medium rectangular domain. The principle direction of the anisotropy is aligned with the coordinate axes. In this case, two points flux approximation is sufficient to solve the system. However, when the anisotropy direction is not aligned with the coordinate system, the two points flux approximation may fails to account for the fact that pressure gradient in one direction can cause flow in other directions. In the case of the presence of full permeability tensor, the more involved multipoint flux approximation (MPFA) methods (as will be explained later) are need in order to obtain the correct discretization. Although similar work have been done by Salama et al. [13], they considered the update of permeability tensor the same in all direction. In this work, we consider the update of permeability different in the different directions which is more realistic. Starting with the governing equation, the mass conservation equation is

$$\nabla \cdot \mathbf{u} = 0 \tag{7}$$

Darcy's law:

$$\mathbf{u} = -\frac{\mathbf{K}}{\mu}\Big(\nabla p - \rho \mathbf{g}\Big) \tag{8}$$

where $\mathbf{K}$ is the permeability tensor, $\mu$ is the fluid viscosity, $\rho$ is the fluid density and $\mathbf{g}$ is the gravity. The transport of nanoparticles in size interval $i$ is governed by ([8], [9])

$$\phi\frac{\partial c_i}{\partial t} + \nabla \cdot \Big(\mathbf{u}c_i + \phi\tau\mathbf{D}\nabla c_i\Big) = R_t + Q_{c_i} \tag{9}$$

Here $c_i$ is the concentration of nanoparticles in interval $i$, $\mathbf{D} = \mathbf{D}^{\text{disp}} + D_i^{Br}$ , where $\mathbf{D}^{\text{disp}}$ and $D_i^{Br}$ are second order tensor that accounts for hydrodynamic dispersion and Brownian diffusion, respectively. They are obtained by the following formula:

$$\mathbf{D}^{\text{disp}} = d_{t,w}|\mathbf{u}|\mathbf{I} + \Big(d_{l,w} - d_{c,w}\Big)\frac{\mathbf{uu}}{|\mathbf{u}|} \tag{10}$$

and

$$D_i^{Br} = \frac{k_B T}{3\pi\mu d_{p,i}}. \tag{11}$$

$R_i$ in equation (9) is the net rate of loss of nanoparticles in interval i. In this work we use the model in Gruesbeck and Collin [10]:

$$R_i = \frac{\partial s_{1i}}{\partial t} + \frac{\partial s_{2i}}{\partial t}. \tag{12}$$

where

$$\frac{\partial s_{1i}}{\partial t} = \begin{cases} \gamma_{di}|\mathbf{u}|c_i, & |\mathbf{u}| \le \mathrm{u}_c \\ \gamma_{di}|\mathbf{u}|c_i - \gamma_{ei}(|\mathbf{u}| - \mathrm{u}_{ci})s_{1i}, & |\mathbf{u}| > \mathrm{u}_c \end{cases}. \tag{13}$$

and

$$\frac{\partial s_{2i}}{\partial t} = \gamma_{pt,i}|\mathbf{u}c. \tag{14}$$

In Eq. (13) $\gamma_{di}$ and $\gamma_{ei}$ are rate coefficients for surface retention and entrainment of nanoparticles in interval $i$, respectively. With equations (13) and (14), the porosity and permeability are updated:

$$\phi = \phi_0 - \sum \delta\phi_i = \phi_0 - (s_{1i} + s_{2i}) \tag{15}$$

$$\mathbf{K} = \mathbf{K}_0\Big[(1-f)k_f + f\frac{\phi}{\phi_0}\Big]^l \tag{16}$$

where $\mathbf{K}_0$ and $\phi_0$ are initial permeability and porosity, $f$ is called flow efficiency factor and is calculated as

$$f = 1 - \gamma_f s_2 \tag{17}$$

# 3 Numerical algorithm

## 3.1 Multipoint flux approximation

The simulation code was written in FORTRAN 95. For spatial discretization, we use multipoint flux approximation (MPFA) method to deal with the porous media whose direction of anisotropy is not aligned with the coordinate system, in which case the permeability tensor is full. In the 2-D problem, the MPFA method builds the interaction region (dashed line, see Fig. 1) that is centered on the four adjacent cells and there are four fluxes need to be calculated in each interaction region. in which each flux is approximated by

$$f \approx \sum_{i\in\Omega} t_i\Phi_i \tag{18}$$

where $t_i$ and $\Phi_i$ are the transmissibility coefficient and the potential gradient (for instance, the pressure gradient) at the center of the cell-$i$, respectively. The set $\Omega$ depends on the dimension of the considered problem. The fluxes are conserved locally by assuming the inflow and outflow fluxes are equal. From Figure 1 the half flux $f_{ij}$ is give by

$$\begin{aligned} f_{ij} &\approx -t_i^{xx}(p_{ij} - p_i) - t_i^{xy}(p_{ik} - p_i) \\ &\approx -t_j^{xx}(p_j - p_{ij}) - t_j^{xy}(p_{jl} - p_i). \end{aligned} \tag{19}$$

The half fluxes $f_{ik}$, $f_{jk}$ and $f_{kl}$ are obtained in a similar fashion. Each flux involves two adjacent cells to be considered as expressed in Equation (18). From each interaction region, we would obtain four systems of equations that need to be solved locally. Each full flux involves two interaction regions and hence six pressure variable in neighboring cells. It is clear that the construction of MPFA stencil is quite complicated. The remedy we use here is to adapt the experimenting field approach developed by Sun et al. [11], which solves a set of local problems and construct the global system automatically (Salama et al.,[12]). In experimenting field approach, the matrix coefficients are obtained by solving several local problems. The predefined experimenting pressure fields are designed and operated over the local problems such that the global matrix coefficients are obtained.

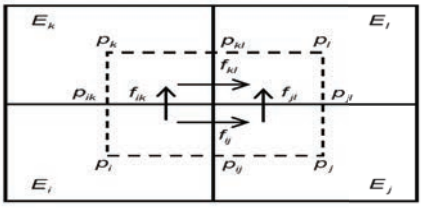


Figure 1

### 3.2 Aggregation-based algebraic multigrid

After the global matrix for solving pressure field is constructed, the linear system is solved by aggregation-based algebraic multigrid method [14]. Due to their $O(N)$ complexity under certain circumstances, multigrid methods have been proved to be one of the most efficient algorithms to solve the elliptic type partial differential equations numerically. As one of the multigrid methods, aggregation-based algebraic multigrid (AGMG) can be very efficient because of its relatively low setup time. However, it may suffer slow convergence in some difficult cases. Specifically, the diffusion equations whose diffusion coefficients contain rotated anisotropy appear to be a challenge problems for aggregation-based algebraic multigrid methods. For this type of the problem, Chen et. al. [15] proposed an improved aggregation strategy to reduce the number of iterations. The new automatic aggregation algorithm determines appropriate aggregates based on eigenvectors associated with small eigenvalues of a block splitting matrix. The improved algorithm was employed in the simulation code.

## 4 Numerical example

In this work we consider a set of 2D numerical experiments to investigate the effects of anisotropy on the transport of nanoparticles. The domain studied is rectangular and consists of three zones, where the middle zone is anisotropic. In addition, the angles between the direction of anisotropy and the $x$-axis considered in the simulations are $0°$, $30°$, $45°$ and $60°$. At the center of the domain, nanoparticles are emitted at the intensity $10^{-6}$ 1/s. The fluid flows advect these particles and certain amount of them deposit in the media. The deposition of nanoparticles changes the heterogeneity of media in a way that the anisotropy ratio decreases with time. All the numerical simulations stop when the anisotropy ratio reduces to 1, i.e., when the media becomes isotropic. For the boundary conditions, we impose the velocity boundary condition of $5 \times 10^{-6}$ m/s on the left edge of the domain. On the right hand boundary the pressure is 1 atmosphere (1.01325 bar). No flow boundary condition is imposed on the top and bottom of the domain. The parameters used in the numerical simulations are listed in Table 1. The nanoparticles are assumed not affecting the flow field. This assumption allows the decoupling of flow and transport equations.

## 5 Results and disscusion

In this work the primary concern is the effect of the anisotropy of the media on various fields, such as pressure, porosity, flow and concentration distribution of nanoparticles. The anisotropy is defined by two parameters. The first parameter is the angle the principle direction of

Table 1: Parameters for single nano-size particle transport simulations.

| Parameters | Values |
|---|---|
| Initial permeability | $\mathbf{K_0}$ |
| Isotropic layer | $\begin{bmatrix} 9.869 & 0 \\ 0 & 9.869 \end{bmatrix} \times 10^{-14}$ m$^2$ |
| Anisotropic layer | |
| 30° | $\begin{bmatrix} 7.649 & 3.846 \\ 3.846 & 3.208 \end{bmatrix} \times 10^{-14}$ m$^2$ |
| 45° | $\begin{bmatrix} 5.428 & 4.441 \\ 4.441 & 5.428 \end{bmatrix} \times 10^{-14}$ m$^2$ |
| 60° | $\begin{bmatrix} 3.208 & 3.846 \\ 3.846 & 7.649 \end{bmatrix} \times 10^{-14}$ m$^2$ |

| Parameters | Values |
|---|---|
| $L_x \times L_y$ | 5 m × 5 m |
| $n_x \times n_y$ | 30 × 30 |
| $\phi_0$ | 0.3 |
| $D^{Br}$ | $2 \times 10^{-9}$ m$^2$s$^{-1}$ |
| $\mu$ | $10^{-3}$ Pa s |
| $\gamma_d$ | 5 m$^{-1}$ |
| $\gamma_{pt}$ | 1 m$^{-1}$ |
| $\gamma_f$ | 0.001 m$^{-1}$ |
| $k_f$ | 0.6 |
| $c_0$ | 0 |
| $c_{s1}$ | 0 |
| $c_{s2}$ | 0 |
| $q_c$ | $10^{-6}$ s$^{-1}$ |
| $t^{\text{simulation}}$ | 129600 s |
| $\Delta_t$ | 3.55 s |

anisotropy is making with the $x$-axis. The other is the anisotropy ratio, which is the ratio between the anisotropy components in the principle directions. We study the scenarios when the deposition of nanoparticles changes the anisotropy ratio of porous media. The deposition also decreases the volume of the void space available for flow and therefore, the permeability also decreases. Since the velocity is set constant at the left boundaries, the average pressure changes as a consequence of the decrease of both anisotropy ratio and permeability with time. In this section we highlight these effects on the different scenarios.

The results of numerical experiments are shown in Figure 2 - 9. Figures 2 - 5 show an update of the various fields after the anisotropy ratio reduced to 1. In these figures the scalar fields and the corresponding velocity fields are presented simultaneously. From Figure 2 we see that the pressure and velocity fields distort with direction of anisotropy. In Figure 3a the pressure and velocity fields slightly deform. As the anisotropy angle increases, the gradient of the pressure profiles along the $x$-direction increases. Figure 6a shows the evolution of the average pressure at the inlet for the different anisotropy angles with time. One first observes that the average pressure at the inlet at the start of simulations is larger the larger the anisotropy angle. This can be attributed to the decrease of effective permeability due to the accumulation of nanoparticles. In order to maintain the constant flux condition at the inlet boundary, the average inlet pressure increases with time because of the decrease of permeability. The large anisotropy angle of the media hinders the flow more severely than the smaller angles do and enhance the deposition process of the nanoparticles. Another interesting effect caused by the flow direction change due to the anisotropy of media is the high concentration of nanoparticles at the top end of the interface between two regions (recall that the whole domain is divided into three regions, with the middle layer contains rotated anisotropy), as seen from Figure 4. With no flow boundary condition, the top boundary acts as a wall so that the flow direction changes rapidly and the accumulation of the nanoparticles becomes sever.

Figure 6b shows the evolution of minimum porosity with time for the different anisotropy

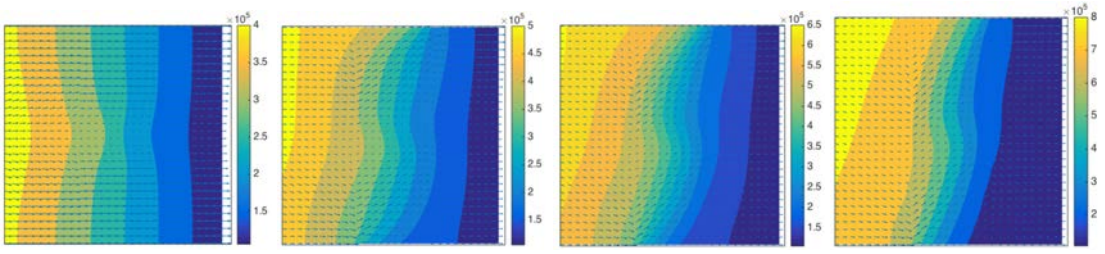

(a) Isotropic (b) 30° (c) 45° (d) 60°

Figure 2: Pressure fields

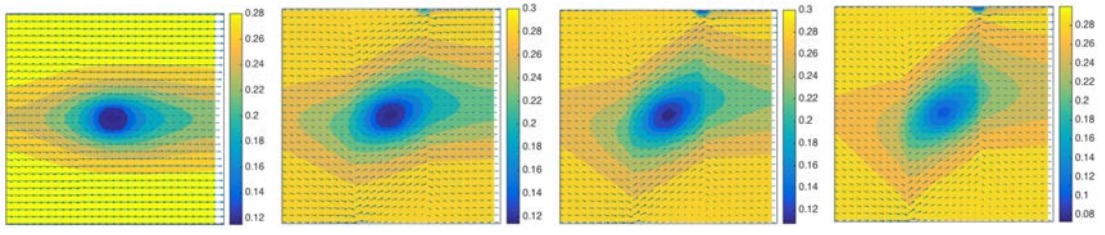

(a) Isotropic (b) 30° (c) 45° (d) 60°

Figure 3: Porosity

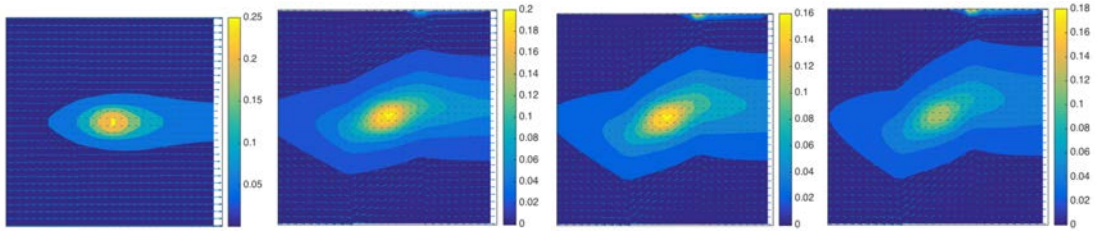

(a) Isotropic (b) 30° (c) 45° (d) 60°

Figure 4: Concentration

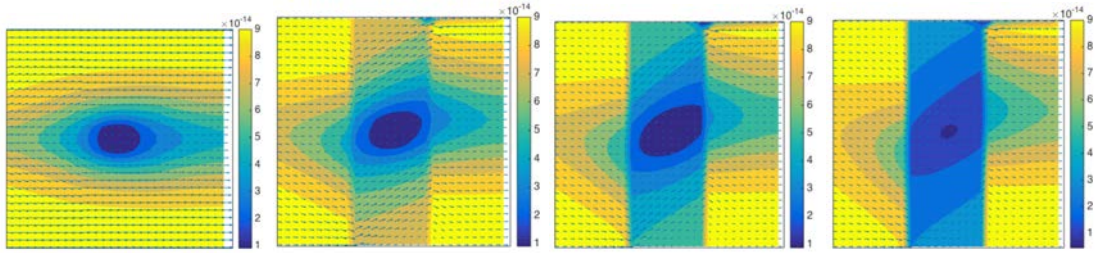

(a) Isotropic (b) 30° (c) 45° (d) 60°

Figure 5: Permeability

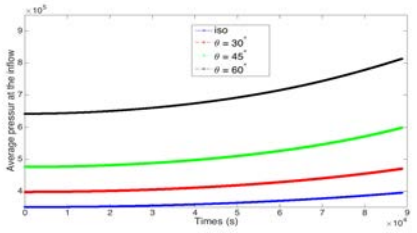


(a) Comparison of the average pressure profile at the inlet for the different anisotropy scenarios.

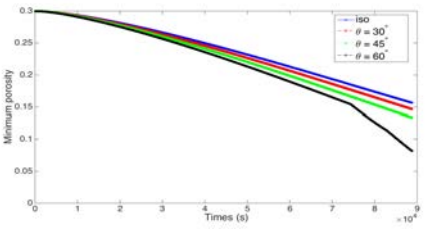


(b) Comparison of the evolution of the minimum porosity profile for the different anisotropy scenarios.

Figure 6

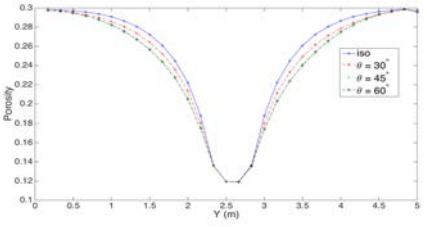


(a) Porosity in the center layer. x = 2.5 m

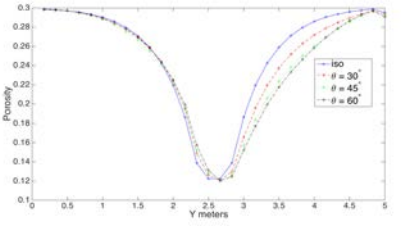


(b) Porosity in the center layer, x = 3.0 m.

Figure 7

scenarios. From this figure it is clear that the minimum porosity decreases with time as a consequence of the increase of deposition of nanoparticles. Furthermore, the minimum porosity curves are different for different anisotropy conditions (porosity is smaller the larger the anisotropy). This is also manifested in Figure 7 which shows profiles of porosities at two $x$-positions along the height of the middle domain after the anisotropy ratio reduced to 1. Figure 7a shows the porosity profile at the center of the middle layer. One notices that the porosities for all scenarios are very closed near the source of the nanoparticles. Away form the source, porosity is the least the larger the anisotropy angle. We also exhibit the porosity profile somewhere in the middle layer but closer to the flow exit, as shown in Figure 7b. The profile deviates toward the direction of anisotropy and the minimum porosities are very closed in all cases. It expectable that the porosity is the least the larger the anisotropy angle, since the direction of anisotropy affects the inlet pressure and the distribution of the deposition of the nanoparticles.

Anisotropy also affects the concentration profile significantly. Figures 4 exhibits the concentration contours for different scenarios. As seen from the figures the nanoparticles spread out in broader range for the case $\theta = 60°$ than in the other scenarios. In the region near the emission source, the concentration is the least the larger the anisotropy angle. This is also manifested in Figure 8a and 8b, which show the comparisons of the concentration profiles along the middle layer height. Based on this figures, the concentration is higher for the isotropic scenario and decreases with the increase of anisotropy. These behaviors (Figures 7 and 8) may possibly be described by exploring velocity profiles as shown in Figures 9a and 9b. Figure 9a shows a comparison between the $x$-component velocity along the height of the middle layer for the different

anisotropy scenarios and it is clear that in the middle of the middle layer, the $x$-component velocity drops because of the decrease in permeability. Meanwhile, the $x$-component velocity is larger the larger anisotropy angle. Similar phenomena is observed in Figure 9b which shows the comparison for the magnitude of velocity along the middle layer height. Again, It is clear that velocity magnitude is larger the larger the anisotropy. This explains the behavior of both the concentration and the porosity in the middle layer, which is manifested by the fact that increasing the velocity increases the dispersion and deposition rate.

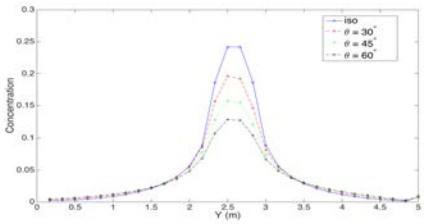


(a) Concentration in the center layer. x = 2.5 m

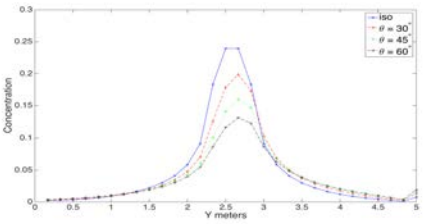


(b) Concentration in the center layer. x = 3.0 m

Figure 8

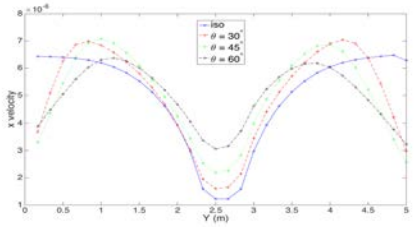


(a) x velocity in the center layer. x = 2.5 m

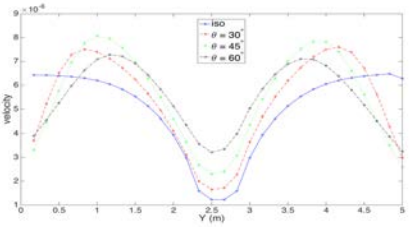


(b) Speed in the center layer. x = 2.5 m

Figure 9

# 6 Conclusion

In this work, we have simulated the flow and transport of nanoparticles in porous media with rotated anisotropy. Spatial variables were discretized using the multipoint flux approximation method. The linear system for solving pressure field arising from MPFA discretization is solved by aggregation-based algebraic multigrid. A source term in the middle of anisotropic domain is used to introduce nanoparticles to the domain. We considered a more realistic mechanism that the anisotropy ratio decreases with time in response to the deposition of nanoparticles. Several scenarios of anisotropy are considered including different anisotropy angles. Since the simulations stop after the anisotropy ration became 1, the time steps used for various scenarios are different. We found that the larger anisotropy angle was, the smaller number of time step was used. This indicates that large angle between the anisotropy and the principle flow direction ($x$-direction) causes faster change in anisotropy ratio. The simulation results and plots for variables (pressure, porosity, velocity and concentration) manifested this observation.

When nanoparticles are deposited into the pore space, they deteriorate both the velocity and permeability fields. Pressure and velocity fields change in response to the change in permeability.

# References


[1] P. R. Johnson, M. Elimelech, *Dynamics of colloid deposition in porous media: blocking based on random sequential adsorption.* Langmuir 11 (1995), 801-812.

[2] J. F. Schijven, S. M. Hassanizadeh, R. H. de Bruin, *Two-site kinetic modeling of bacteriophages transport through columns of saturated dune sand.* J. Contam. Hydrol. 57 (2002), 259 - 279.

[3] S. A. Bradford, S. R. Yates, M. Bettahar, J. Simunek, 2002. *Physical factors affecting the transport and fate of colloids in saturated porous media.* Water Resour. Res. 38 (2002), 1327 - 1338

[4] E. Goldberg, M. Scheringer, T. D. Bucheli, K. Hungerbhler, *Critical assessment of models for transport of engineered nanoparticles in saturated porous media.* Environ. Sci. Technol. 48 (21), 2014, 12732 - 12741.

[5] A. Benamar, N. D. Ahfir, H. Q. Wang, A. Alem, *Particle transport in a saturated porous medium: pore structure effects.* C. R. Geosci. 339 (2007), 674 - 681

[6] F. He, M. Zhang, T. Qian, D. Zhao, *Transport of carboxymethyl cellulose stabilized iron nanoparticles in porous media: column experiments and modeling.* J. Colloid Interface Sci. 334(2009) , 96-102.

[7] E. Cullen, D. M. O'Carroll, E. K. Yanful, B. Sleep, *Simulation of the subsurface mobility of carbon nanoparticles at the field scale.* Adv. Water Resour. 33 (2010), 361-371.

[8] M. F. El-Amin, S. Sun, A. Salama, *Enhanced oil recovery by nanoparticles injection: modeling and simulation.* SPE-164333. SPE Middle East Oil and Gas Show and Exhibition Held in Manama, Bahrain, March 2013.

[9] M. F. El-Amin, A. Salama, S. Sun, *Numerical and dimensional analysis of nanoparticles transport with two-phase flow in porous media.* J. Petrol. Sci. Eng. 128 (2015), 53-64.

[10] C. Gruesbeck, R. E. Collin, *Entrainment and deposition of fine particles in porous media.* Soc. Pet. Eng. J. 24(1982), 847?855.

[11] S. Sun, A. Salama, M. F. El-Amin, *An equation-type approach for the numerical solution of the partial differential equations governing transport phenomena in porous media.* Procedia Comput. Sci. 9 (2012), 661?669.

[12] A. Salama, S. Sun, M. Wheeler, *Solving global problem by considering multitude of local problems: application to flow in anisotropic porous media using the multipoint flux approximation.* J. Comput. Appl. Math. 267 (2014), 117?130.

[13] A. Salama, S. Sun, M. Wheeler, *Numerical investigation of nanoparticles transport in anisotropic porous media.* J. Contaim. Hyro., 267 (2014), 117-130.

[14] Y. Notay, *AGMG: Iterative solution with AGgregation-based algebraic MultiGrid*, http://homepages.ulb.ac.be/ynotay/AGMG.

[15] M. Chen, A. Greenbaum, *Analysis of an aggregation-based algebraic two-grid method for a rotated anisotropic diffusion problem*, Numer. Lin. Alg. with Appl., Vol. 22, Issue 4, Aug. 2015, pp. 681-701.